J Mater Sci (2007) 42:1561–1576
DOI 10.1007/s10853-006-0987-6

Nanoparticle consolidation using equal channel angular extrusion at room temperature

I. Karaman · M. Haouaoui · H. J. Maier

Received: 17 June 2006 / Accepted: 21 September 2006 / Published online: 4 January 2007

Abstract In the present work, we demonstrate the use of equal channel angular extrusion (ECAE) for the consolidation of metallic nanoparticles *at room temperature* as a bottom up approach to fabricating nanocrystalline (NC) metals. Three different initial average particle sizes of pure copper were used: –325 mesh micron size particles, 130 nm and 100 nm nanoparticles. The processing work was divided into three major stages (Stages I–III), depending on the powder filling procedure used prior to ECAE, to investigate the effect of processing parameters such as extrusion rate and ECAE route, powder filling environment, and hydrostatic pressure on the final performance of the consolidates. Microstructure of the consolidates and monotonic mechanical behavior were determined at room temperature. The Stage I experiments revealed what can materials, ECAE routes and range of extrusion rates to use for achieving near full density consolidates. In Stages II and III, the effect of initial compact density on the resulting mechanical behavior was investigated. It was found that the prior compaction is helpful in breaking down the initial nanoparticle agglomerates and achieving high tensile strength and ductility levels in the ECAE consolidates. Tensile strength as high as 800 MPa and tensile ductility as high as 7% were achieved in 100 nm Cu particle consolidates, which were more than 1.5 cm in diameter and 10 cm in length, with a bimodal grain size distribution in the range of 50–100 nm and 300 nm–600 nm. ECAE was also used to consolidate 316 L stainless steel nanoparticles resulting in bulk samples with tensile strength of 1180 MPa and 4% ductility. The present study shows that ECAE can be a feasible method for fabricating bulk NC materials with all dimensions in the centimeter range. Future work is needed to further optimize the processing parameters for improving the ductility level further and controlling the grain size distribution.

I. Karaman (✉) · M. Haouaoui
Department of Mechanical Engineering, Texas A&M University, College Station, TX 77843, USA
e-mail: ikaraman@mengr.tamu.edu

H. J. Maier
Lehrstuhl für Werkstoffkunde, University of Paderborn, 33098 Paderborn, Germany

Introduction

Materials with ultra-fine grains and nanostructures (<100 nm) have attracted considerable interest because of their unique properties compared with conventional materials [1–33]. The main challenge of using nanocrystalline (NC) materials in structural applications is to fabricate them in *bulk* and control processing-induced defects with the purpose of reaching ultra high strength and ductility combinations. The development of novel severe plastic deformation (SPD) techniques has made bulk structural materials (with centimeter dimensions) of very fine grain size and extraordinary strength a reality. Equal channel angular extrusion (ECAE) and high-pressure torsion (HPT) are the most well known SPD methods. Other techniques for producing bulk NC materials include: (1) crystallization from amorphous phases [34, 35], (2) the mechanically activated self-heat sustaining reaction method [36, 37], (3) mechanical alloying followed by

compaction and sintering [30, 38–45], (4) compaction and sintering of nanopowders produced by evaporation-condensation techniques [46–48], (5) electrodeposition [17, 18, 49–52], and (6) plasma sintering [53–56]. Each method has advantages and disadvantages. For instance, it is difficult to obtain grain sizes less than 100 nm using ECAE when starting from bulk coarse grained materials [57–68]. The sample sizes that can be obtained by HPT and hot compaction of nanopowders are very small and microstructural uniformity is an issue [58, 69, 70]. Samples produced via electrodeposition are often contaminated by hydrogen, carbon and sulfur [6, 17, 18, 21, 29, 52]. Bulk amorphous materials are still difficult to make, and thus, crystallization of amorphous metals may not be the optimal method for fabricating bulk NC materials [34, 35]. Clearly, comparison between the various nanomaterials fabricated using different processing routes is not straight forward, since there can be significant differences in microstructural homogeneity, local chemistry, impurity concentration and distribution, porosity and sample size.

The consolidation of powders via ECAE at low temperatures makes it possible to fabricate bulk materials with grain sizes from the nano to micron size scale [66, 71–74]. In ECAE, load is applied to a powder filled can in the inlet channel and the billet is deformed (powder consolidated) as it passes through the shear zone and is extruded from the horizontal channel as shown schematically in Fig. 1. The benefit of powder consolidation by ECAE is effective consolidation at lower temperatures than normally required by HIP operations [57, 71–74]. ECAE processing is especially attractive for NC materials because of (1) the possibility of consolidation below dynamic recovery temperatures, (2) large product cross-sections, and (3) easy incorporation of second phase components (other powder, filamentary, or wire/rod dispersoids), which are not suitable for incorporation during a melting step. ECAE powder consolidation offers additional benefits as compared to conventional extrusion powder consolidation since multiple passes are possible in ECAE without changing the cross-section which should lead to a better consolidation. ECAE also permits a variety of deformation configurations by changing the orientation of the billet with respect to the extrusion axis after each pass [75–77]. In comparison with conventional extrusion, the same amount of equivalent strain can be achieved with lower extrusion loads in ECAE using a novel tool design incorporating moving die walls [78–80]. For details on the nomenclature used in ECAE processing, see [58, 81].

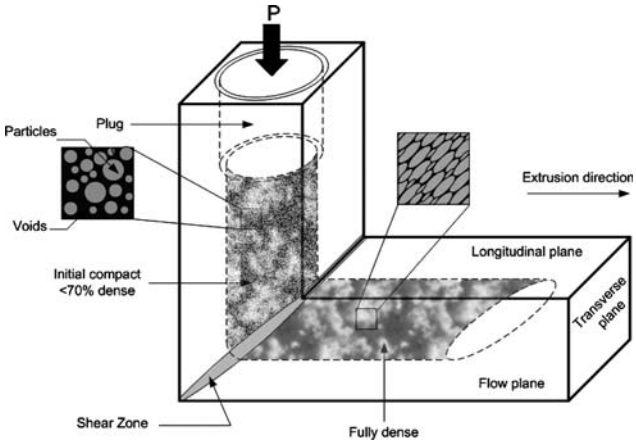

Fig. 1 Schematic of the ECAE powder consolidation process

Work on ECAE consolidation of micropowders began at Texas A&M University in the mid 90s [66, 71, 72, 81–89]. Materials successfully consolidated have included Al-6061, pure Cu, Cu blended with Ag, Sn–8Cu blended with Al_2O_3 and SiO_2, NbFeB blended with 304 stainless steel or pure Cu, WC blended with Co, and amorphous Cu-, Fe-, Hf- and Zr-based alloys [81–89]. In all cases (except for the Sn alloy blends containing SiO_2), consolidation to a density above 99% of the theoretical value has been achieved with one or two ECAE passes.

The primary challenges during consolidation of nanoparticles are the retention of a nanograin size and the elimination of residual porosity. Heterogeneities such as large pores and abnormal grains often persist in the final microstructure and have a significant influence on properties [29, 90–92]. Because of the agglomerate formation in loose nanoparticles and compacts, pore distributions become bimodal with two types of pores: small intercrystallite pores with dimensions approximately equal to the particle size and large interagglomerate pores [93]. Closure of large pores needs an active plastic flow of material at a level larger than the size of nanoparticles. Macroscopic shear provides this kind of flow. Damage development proportional to accumulated shear strain can be suppressed with a high level of hydrostatic pressure during processing. In ECAE, shear deformation is inherent to the process and hydrostatic pressure comes from canning and/or back pressure. In the present work, the size of agglomerates varies from few microns up to hundreds of micron as shown in Fig. 2a. The mixture of these agglomerates definitely creates a range in porosity distribution and elimination of porosity to obtain full density becomes a challenge for obtaining NC metals with high strength and ductility.

The presence of surface oxides poses a different kind of challenge when consolidating nanoparticles.

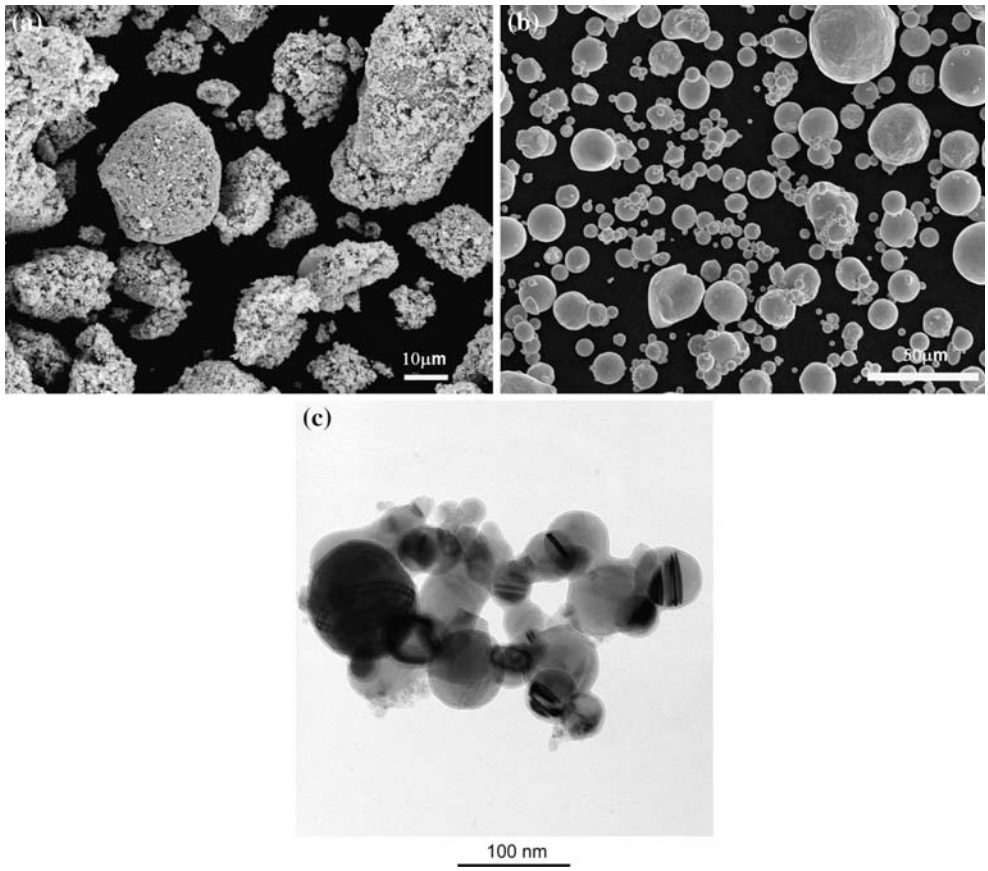

Fig. 2 SEM images of (**a**) the agglomerates of 130 nm Cu particles and (**b**) –325 mesh Cu powder. (**c**) A bright field TEM image of the 130 nm Cu particles

This is because, their content is much higher in nanoparticles and proper binding by diffusion requires that they be broken by a suitable combination of stresses and temperature. In our previous work on the ECAE consolidation of amorphous particles [87, 88], it was possible to break the surface oxide layers during the first ECAE pass. In the present work, even though we have not conducted a detailed analysis on whether the oxide layers were effectively broken, it is believed that they were not a major problem given the tensile ductility levels achieved. The remnant porosity along the inter-agglomerate boundaries was the main factor dictating the ductility levels. Moreover, broken oxides can be beneficial in suppressing grain growth as shown in consolidated cryomilled Al particles using conventional extrusion [38, 39].

In this study, Cu particles with three different average particle sizes (–325 mesh, 130 nm and 100 nm) were consolidated using ECAE at room temperature. The processing work was divided into three stages depending on the powder filling procedure and initial powder compaction method prior to ECAE. Here, we report on the microstructural evolution of powder consolidates and room temperature mechanical response after each stage. We also discuss how each stage led us to select better processing parameters such as extrusion rate and ECAE route, hydrostatic pressure level through the selection of the powder can material, and powder filling environment. Moreover, we present some preliminary results on the ECAE consolidation of 316L stainless steel nanoparticles to show the applicability of this process to other materials. Finally, we propose few strategies for further enhancement of plastic strain at fracture while maintaining high strength levels.

Experimental procedures

Copper powders with three different sizes (–325 mesh, 100 and 130 nm), and 316 L stainless steel (SS) powder (100 nm) were processed in this study. U.S. DOE Ames Laboratory provided the gas atomized –325 mesh Cu powder, while Cu and SS nanoparticles were acquired from Argonide Corporation, Sanford, Florida. Nanoparticles were fabricated using the electroexplosion of wire process (EEW) [94]. The oxygen content of the Cu nanoparticles was measured to be 0.11 wt% using Fast Neutron Activation Analysis. 2.5 centimeter square cans were used to contain the

powder during consolidation. The exact dimensions of the powder space and the materials of the cans are summarized in Table 1. A 2.5 centimeter long solid can material was left at the leading and trailing edges of the cans to eliminate the non-uniformly deformed regions in the consolidates.

We have divided this study to three major processing stages depending on the filling procedure and powder compaction method prior to ECAE: manual tapping of filled powder (Stage I), hand pressing during filling (Stage II), and cold isostatic pressing (CIP) (Stage III). The main goal of using three different filling procedures was to determine how effective each procedure is on minimizing the effect of nanoparticle agglomeration and bimodal porosity distribution on the final consolidation performance. Moreover, it was intended to reveal whether only manual tapping would be sufficient to achieve near full density via ECAE. Stainless steel powders were only studied in Stage I. The two later stages were also motivated by the desire to achieve higher material yield (the final consolidate length) after consolidation. The applied pressure during hand-pressing was 10 ksi and CIPing pressure was 40 ksi. In Stage II and for one case in Stage I, we calculated the density of the filled powder measuring the powder weight and the volume of the powder space in the cans. The green density of the manually tapped –325 mesh Cu powder was about 62 ± 2% while that of hand-pressed nanoparticles (either 130 or 100 nm) was about 49 ± 3%. The density was about 45% for the hand-pressed 50 nm particles (not presented here). This shows that initial particle size makes a significant difference in the compact density due to nanoparticle agglomeration. For micron size particles, hand-pressing do not cause any significant change in the initial compact density as compared to manual tapping. Manual tapping results in the lowest and CIPing should normally give the highest initial compact density.

Three different can materials were used: 1018 steel, nickel and copper. In Stage I, some of the filling was conducted manually in air for the 100 nm Cu particles, which was loaded into nickel or steel cans to compare the effect of can material on consolidation. The consolidates in nickel cans showed much better integrity than the ones in the steel cans, therefore, for the rest of the study, nickel was the choice of can material for Cu nanoparticles. For all the other cases, the cans were degassed in vacuum for 8 h after the filling. The –325 mesh powder was degassed at 150 °C while the degassing temperature was 130 °C for the nanoparticles. Copper cans were used for the –325 mesh Cu

Table 1 Summary of the processing conditions used for the ECAE consolidation of micron and nanometer size Cu particles and 316 L stainless steel nanoparticles. All the Cu particles were consolidated at room temperature

Stage	Case#	Route	Can specifications (material/length of powder space)	Filling environment	Powder size
Stage 1: Manual tapping	1	1A	Nickel/5 cm	Air	100 nm
	2	2C	Nickel/5 cm	Air	
	3	1A	Steel 1018/10 cm	Air	
	4	2A	Steel 1018/10 cm	Air	
	5	2C	Steel 1018/10 cm	Air	
	6	1A	Steel 1018/10 cm	Air	
	7	2A	Nickel/10 cm	Air	
	8	2C	Nickel/10 cm	Air	
	9	1A	Copper/7.6 cm	Vacuum at 150 °C	–325 mesh
	10	2A	Copper/7.6 cm	Vacuum at 150 °C	
	11	2B	Copper/7.6 cm	Vacuum at 150 °C	
	12	2C	Copper/7.6 cm	Vacuum at 150 °C	
	13	4C	Copper/7.6 cm	Vacuum at 150 °C	
	14	2B	Nickel/7.6 cm	Vacuum at 130 °C	130 nm
	15	2C	Nickel/7.6 cm	Vacuum at 130 °C	
	16	4E	Nickel/7.6 cm	Vacuum at 130 °C	
	17	6E	Nickel/10 cm	Vacuum at 130 °C	
	18	4C'	Nickel/10 cm	Vacuum at 130 °C	
	19	2B	316L SS /10 cm (extrusion at 700 °C)	Vacuum at 150 °C	100 nm (SS)
Stage 2: Hand pressing	23	2A	Nickel/10 cm	Vacuum at 130 °C	130 nm
	24	2B	Nickel/10 cm	Vacuum at 130 °C	
	25	4B	Nickel/10 cm	Vacuum at 130 °C	
	26	4C'	Nickel/10 cm	Vacuum at 130 °C	
Stage 3: Cold isostatic pressing	27	4B	Nickel/13 cm	Vacuum at 130 °C	100 nm

powder because of its lower flow strength. As a rule of thumb, one should select the can material such that is has similar flow characteristics as the powder inside the can. Thus, 316 L SS cans were used for the stainless steel powder in the present study.

Note that the requirement for canning or initial compaction of powders in conventional ECAE may be eliminated using back pressure at the exit channel of ECAE die as proposed by Xia and Wu [73]. Back pressure can also improve the uniformity of deformation by making the shear zone more confined, especially if the channel intersection corners are not sharp and there is an associated fan angle. Moreover, higher hydrostatic pressure levels from back pressure can provide more effective consolidation. However, the lack of initial compaction would reduce the material yield, i.e. the length of consolidates would be less. Moreover, unless the whole ECAE system is sealed and in vacuum or inert gas environment, powder encapsulation and evacuation of the cans are necessary to minimize oxidation of particles even with back pressure. This is particularly important for nanoparticles in which oxidation is detrimental.

The filled cans were electron beam welded under vacuum and processed with different ECAE routes under an extrusion speed of 2.5 mm/sec. This speed was selected after comparing the densities of Cu micropowders consolidated using one ECAE pass at different extrusion speeds [95]. Some of the billets were processed using route A (no rotation of the billet between successive passes). The billet is rotated ±90° after each pass for route B (also sometimes referred to as B_A in the literature), +90° and 180° after each pass for routes C' (also known as B_C) and C, respectively. Route E is a 2C extrusion followed by a 90° rotation and then another 2C extrusion. Table 1 summarizes the experimental conditions for each can.

Dog-bone-shaped flat tensile specimens with nominal dimensions of $8 \times 3 \times 1.5$ mm^3 in the gage section and compression specimens with nominal dimensions of $4 \times 4 \times 8$ mm^3 were cut by electrical discharge machining (EDM) along the long axis of the consolidates (the extrusion direction). The surfaces were polished to remove the EDM affected layer. Experiments were performed at room temperature with a hydraulic MTS test frame under a strain rate of 5×10^{-4} s^{-1}. The strain was measured with a miniature extensometer (3 mm gage length) mounted on the specimens in both tension and compression experiments. Teflon tape was used in between compression platens and the compression specimens to minimize friction. Neither buckling nor barreling was observed on specimens after compression. Two to three experiments were conducted on companion specimens to check the repeatability of the results.

Transmission electron microscopy (TEM) was employed to study the dislocation arrangements after ECAE processing. For TEM analysis, specimens were prepared by mechanical grinding and twin jet electropolishing. Relatively large electron transparent areas were obtained in Cu samples with a solution consisting of 250 mL phosphoric acid, 500 mL distilled water, 250 mL ethanol, 50 mL propanol and 5 g urea when used at a temperature of –16 °C and a voltage of 15 V. For stainless steel, a solution of 5% perchloric acid in ethanol was used at –20 °C and 15 V. The resulting thin foils were examined in a PHILIPS CM 200 electron microscope operated at 200 kV. X-ray analyses [96, 97] were also performed using a Bruker-AXS D8 diffractometer with Cu K_α radiation to determine the average grain sizes of the consolidated Cu powders in Stage I using the Warren–Averbach method. In the later stages, we have used TEM to determine average grain sizes using both low and high magnification images.

The densities of the consolidated samples were determined in Stage I using Archimedes' principle, according to the ASTM specifications for density measurements of porous materials [98]. Relative densities are based on the measured values and the theoretical density. For other stages, the density was not measured since the processing parameters used usually resulted in more than 99% theoretical density. Instead tensile ductility was used to evaluate the success of the consolidation. In addition, Scanning Electron Microscopy (SEM) was used to examine the fracture surfaces of the tensile specimens.

Experimental results and discussion

Powder characterization and Stage I processing runs

The morphology and size of the Cu particles were determined prior to consolidation. SEM micrographs show that the size of microcrystalline Cu powder ranges from approximately 1 to 10 μm (Fig. 2b). Nanoparticles have the tendency to cluster into agglomerates of bigger size to minimize their surface energy (Fig. 2a). TEM images (Fig. 2c) indeed show the actual morphology and size of the powder: most Cu particles are about 100–130 nm and they have spherical morphology. By comparison, X-ray analyses yielded values of 4.2 μm and 130 nm as grain sizes for the –325 mesh and 130 nm powders, respectively, and 100 nm for the other Cu and

316 L stainless steel nanoparticles used in this study (Tables 1 and 2).

The first phase of Stage I was a preliminary study to determine the appropriate canning materials and extrusion parameters for consolidation of nanoparticles (cases 1–8 in Table 1). The Ni and AISI 1018 steel cans were filled with 100 nm Cu powder in air and manually tapped. The presence of cracks in the AISI 1018 steel cans after the first pass lessened the possibility of successful subsequent extrusions. The final density of specimens from steel cans was therefore low in some cases [66]. A high extrusion speed (25 mm/sec) was also used in a few cases and led to poor consolidation as the final density was on the order of 70% of the full density after one pass. The density values for lower extrusion speeds (2.5 mm/sec and lower) were much higher usually more than 93% up to 99% depending on the can material and number of passes. These preliminary experiments showed the importance of the choice of canning material and extrusion rate for an acceptable consolidation. Nickel was chosen as the canning material for the consolidation of nanoparticles in the remaining Stages II and III. Note that the can material and its flow strength is important since it dictates the amount of hydrostatic pressure on the enclosed powder.

Microstructural evolution and monotonic stress–strain response of consolidated microcrystalline powders

Figure 3 shows the microstructure of the consolidated –325 mesh Cu powders obtained via different ECAE routes after filling the cans, manually tapping, and vacuum outgassing at 150 °C for 8 hours. The TEM foil normals were sectioned perpendicular to the longitudinal plane shown in Fig. 1. The 2A and 2B ECAE consolidates show large areas with low dislocation density. The grains are well developed and are almost free from dislocations in some cases. The microstructure in the 2C sample is more homogeneous but contains high dislocation density regions without clear subgrain formation. Sample 4C exhibits well developed subgrains with relatively thick subgrain boundaries with a high dislocation density. Most of the grain boundaries are clearly visible indicating substantial misorientation between grains. Note, however, that some of them are poorly defined.

Figure 4 presents the tension and compression true stress–true strain response of consolidated –325 mesh Cu powder. As can be seen in the figure, one ECAE pass was not sufficient for complete consolidation and both tension and compression specimens fractured prematurely. Compression specimens exhibited a high ultimate strength level of 480 MPa and good ductility (except the sample from Route 1A). All compression experiments were stopped at a strain of 10% because of considerable shape change. The best tensile response was observed in the sample consolidated using route 2B, which exhibited significant true strain at fracture (19.2%) for an ultimate true tensile strength of 470 MPa. ECAE 2A and 2C samples showed small strains at fracture while the ECAE 4C sample exhibited a final true strain of 6%. Near elasto-plastic tensile response of the 2B and 4C samples is interesting to note as it contradicts the Considere criterion, which describes the onset of plastic instability [92]. For a true elasto-plastic behavior, necking should start right after the onset of yielding. However, no significant necking was observed in the fractured tension samples. The

Table 2 Summary of the percent theoretical density, measured grain sizes and tensile properties in the –325 mesh and 130 nm Cu particles consolidated using ECAE at room temperature after filling the powder cans in vacuum, manual tapping, outgassing and sealing the cans

ECAE Route	Case #	Powder size	Percentage density (%)	Grain Size		Tension (Extrusion direction)		
				X-Ray	TEM	σ_y (0.2%) (MPa)	σ_{UTS} (MPa)	ε_f (%)
1A	9	–325 mesh (4.2 μm from X-Ray)	97.4	–	–	–	–	–
2A	10		98.3	315 nm	200–300 nm (some grains >500 nm)	406	420	1.9
2B	11		99	300 nm	200–300 nm (some grains <100 nm)	433	470	19.2
2C	12		98.8	250 nm	200–300 nm	–	409	0.5
4C	13		99	260 nm	250 nm	418	443	6.0
2B	14	130 nm (from X-Ray, about	96	110 nm	70–100 nm	690	730	1.2
2C	15	100 nm from TEM)	96	140 nm	~200 nm and 50–80 nm	–	–	–
4E	16		97	–	~250 nm and 40–80 nm	516	546	0.9

σ_y: 0.2% offset yield strength, σ_{UTS}: ultimate tensile strength, and ε_f: strain at fracture

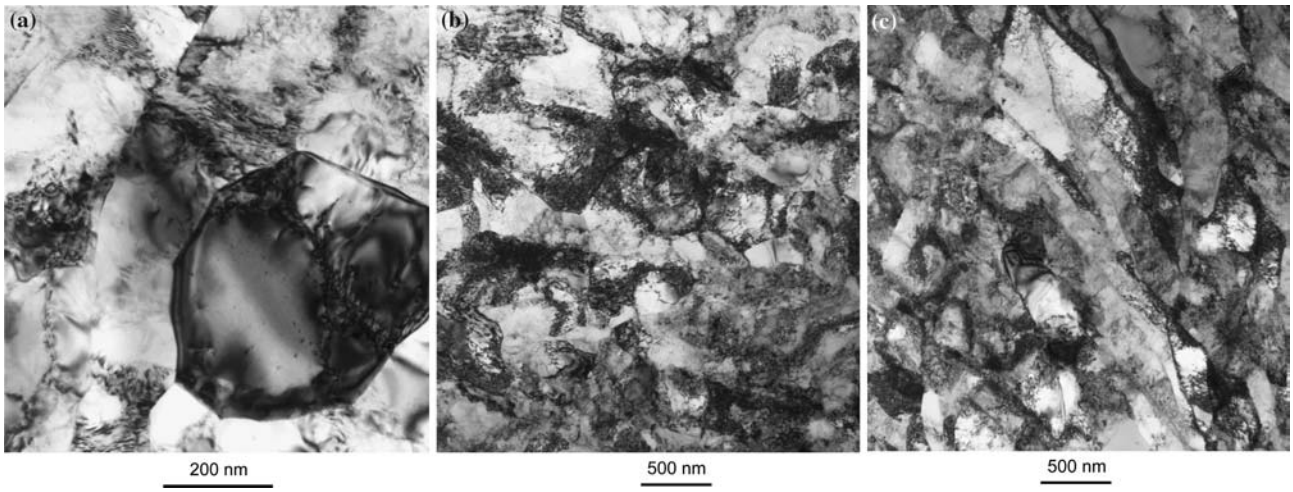

Fig. 3 Bright field TEM micrographs of ECAE processed –325 mesh Cu powder following the routes: (**a**) 2B, (**c**) 2C, and (**d**) 4C. The foil normal is perpendicular to the longitudinal plane shown in Fig. 1

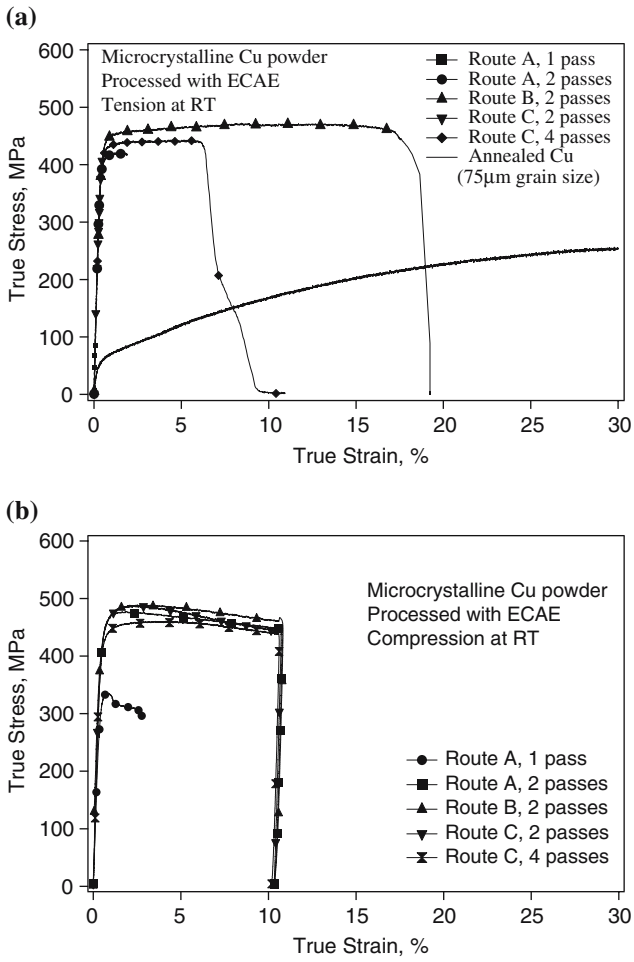

Fig. 4 Room temperature tension (**a**) and compression (**b**) true stress–true strain response of consolidated –325 mesh Cu powder. Recompiled from Ref. [66]

stress levels achieved are similar to what bulk ECAEd Cu samples, with initial coarse grains, usually demonstrate irrespective of the number of passes they experience, *i.e.* ultimate tensile strength levels of around 450 MPa [66, 99].

The near-perfect elasto-plastic behavior was also shown in a recent study by in conventional extrusion consolidated nanosized Cu particles (50 nm). These authors suggested that the mechanical instability criteria for nanocrystalline materials should be revisited since the observed near-perfect elasto-plastic behavior is in contradiction with the Considere criterion. The present results support these findings, however, our average grain sizes are considerably larger than the nanometer range (Fig. 3 and Table 2). It can be argued that near-perfect elastoplasticity is partly due to the combined effect of the bimodal microstructure and the residual porosity. Larger grains in the bimodal structure (Fig. 3) lead to strain hardening but softening caused by residual porosity compensates the hardening. Similarly, strain hardening can also be balanced by a recovery mechanism such as absorption of dislocations by grain boundaries since the structure is heavily deformed. Before necking starts due to the deformation in larger grains, residual porosity may cause fracture.

It should be mentioned that in the study by Champion et al. [92], the average grain size was reported to be 80 nm although the TEM images mostly showed subgrains around 80 nm with purely defined boundaries. The grains with high angle grain boundaries seemed to be more on the order of 200–300 nm in size. The reported mechanical test results support the

latter size range as the ultimate tensile strength levels were around 450–500 MPa which is similar to what ECAE processed bulk Cu usually exhibits with grain sizes of 200–300 nm. However, the reported 80 nm average grain size would have been expected to result in much higher strength levels. The contamination level of nanoparticle consolidates should not be much less than commercially pure Cu, reducing the possibility of attributing such low strength levels to low contamination level. It can be argued that the conventional extrusion consolidation most likely caused abnormal grain growth during consolidation and thus, a bimodal grain size distribution, leading to such low strength levels and near elasto-plastic response.

From the Stage I investigation on the consolidation of the microcrystalline Cu particles, it was concluded that route B results in the best consolidation performance, i.e. very good tensile ductility, and two ECAE passes were sufficient to reach near full density in this route. This finding is reasonable because in route B, orthogonal rotations of billets in successive passes cause more effective close up of pores or cavities left out from the previous passes than what is experienced in routes C or A. In route A, since the shear is applied almost on the same plane in successive passes, it is difficult to close up the pores as this requires some cross-shearing. In the case of route C, the cross shearing after the 180° rotation can cause opening of the pores which are not closed completely in the previous pass. This is thought to be the reason why route C always results in the poorest tensile ductility in consolidates.

Macro and microstructure of consolidated Cu nanoparticles in Stage I

A macrograph of the consolidated 130 nm Cu powder following route 4E is shown in Fig. 5 on the transverse plane. These nanoparticles were filled into the cans, manually tapped and vacuum outgassed at room temperature for 8 hours (Stage I, case#16). The image shows the lack of large cavities and the integrity of the can and enclosed powder maintained during ECAE. We can distinguish flow lines separating regions reflecting different levels of hue seemingly corresponding to areas having dissimilar microstructures. Optical micrographs were taken from different areas of this section to build a qualitative understanding of the prior agglomerate behavior during the extrusion process.

Figure 6 shows the low magnification optical micrographs of the above consolidate. The elongation of the agglomerates along certain flow lines can be clearly seen

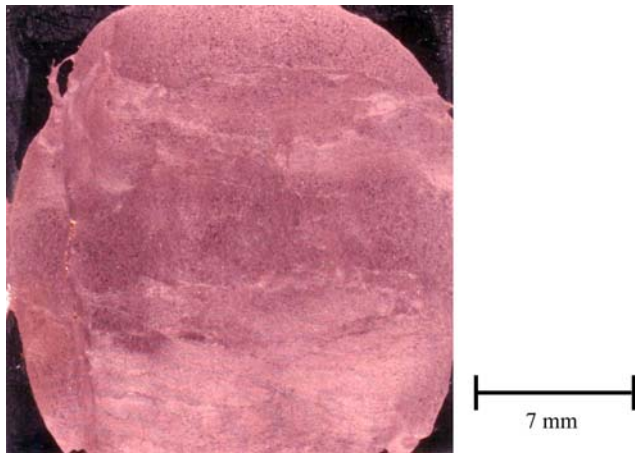

Fig. 5 Cross section of the ECAE consolidated 130 nm Cu powder parallel to the transverse plane (Fig. 1) which was processed following route 4E (case #16 in Table 1). The section was mechanically polished and etched. Dark corners are from the Ni can. Part of the Ni can was machined down before the picture was taken

in Fig. 6. These flow lines do not seem to follow a specific direction but rather organize into blocks of uniform structure. These blocks flow with respect to each other during the extrusion and can be separated by a fine interface as seen in Fig. 6a or by a thicker transition zone as in Fig. 6b. These areas are generally continuous, but in some instances can be the preferred site of discontinuity where microporosity emerges as indicated with an arrow in Fig. 6b. In some cases, three flow regions were observed to intersect at an area (similar to triple junctions at grain boundaries) which is often a strong candidate for the existence of remnant porosity (Fig. 6c). Higher magnification micrographs show that debonding may even occur between agglomerates flowing in the same direction (Fig. 7a). It can be argued that route E contributes to opening the gap between distinct agglomerates during the 180° rotation at the second pass similar to route C. These agglomerates are disintegrated to a certain extent but a considerable proportion is reticent to a break down even after subjecting the can to four passes following routes C and E. Figure 7b shows a fairly large agglomerate etched to reveal the very fine structure due to the nanoparticles.

TEM micrographs of the consolidated 130 nm Cu powder following route C (case #15, Fig. 8a) show that the microstructure is relatively uniform with some large grains in the upper submicron range. The grains are mostly equiaxed and separated by high-angle boundaries. A higher magnification TEM image (Fig. 8b) demonstrates a uniform distribution of the grains less than 80 nm with a fairly narrow grain size

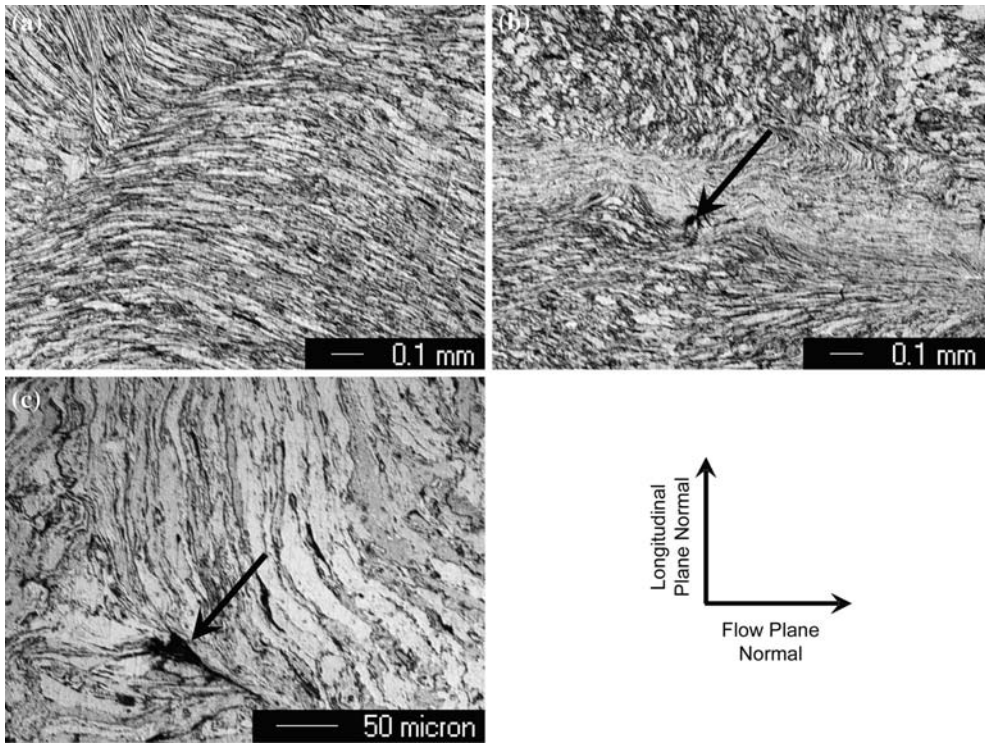

Fig. 6 Low magnification optical micrographs of ECAE consolidated 130 nm Cu powder following route 4E illustrating the flow lines formed by the elongation of powder agglomerates during extrusion

distribution. Similarly, Fig. 8c from the consolidated 130 nm Cu powder following route B demonstrate the presence of very fine grains (about 60–80 nm). The larger light gray areas in the figure with a small change of contrast indicate a low misorientation between small subgrains. Thus, these samples and other consolidated nanoparticles following different routes essentially have a bimodal grain size distribution, which is desired for improving the tensile ductility. Average grain sizes of the consolidates were also determined using X-ray diffraction analyses in Stage I. The values are reported and compared to the grain sizes obtained from several representative TEM micrographs in Table 2.

The consolidated Cu nanoparticles in stage I exhibited much higher tensile strength levels (Table 2) than that of consolidated microcrystalline particles and ECAEd bulk Cu [66], except the ones consolidated using routes A and C. The tensile strength level in the route 2B (case #14) sample, 730 MPa, was exceptionally high, which is about 60% more than that of ECAEd bulk Cu. However, the samples showed limited ductility (1.2%) (Table 2) despite their bimodal grain size distribution. The fracture without substantial ductility in the consolidated 130 nm Cu particles can be attributed to the remnant porosity and to premature debonding between agglomerates. The fracture surface in Fig. 9 suggests that the fracture may initiate due to interagglomeratee debonding. The arrows in Fig. 9 show potential sites for such debonding which are thought to be prior agglomerate boundaries because of their size.

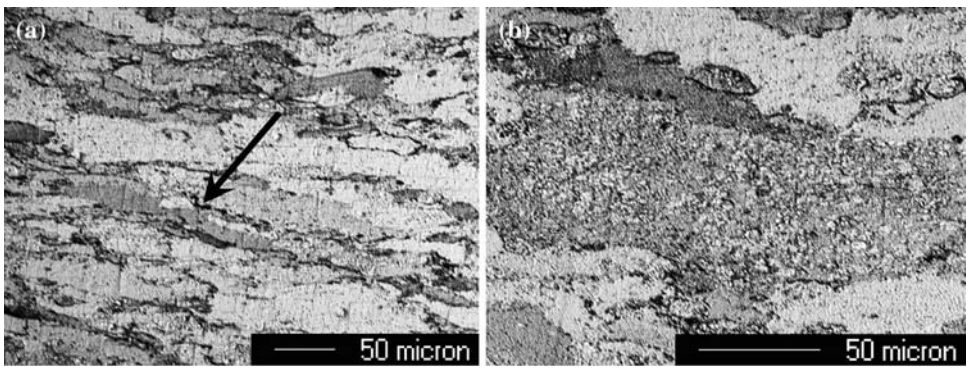

Fig. 7 (**a**) Remnant porosity between similarly deformed nanoparticle agglomerates in the ECAE consolidated 130 nm Cu powder following route 4E due to the 180° rotations in between certain number of passes in route E. (**b**) A very fine microstructure exists in the nanoparticle agglomerates

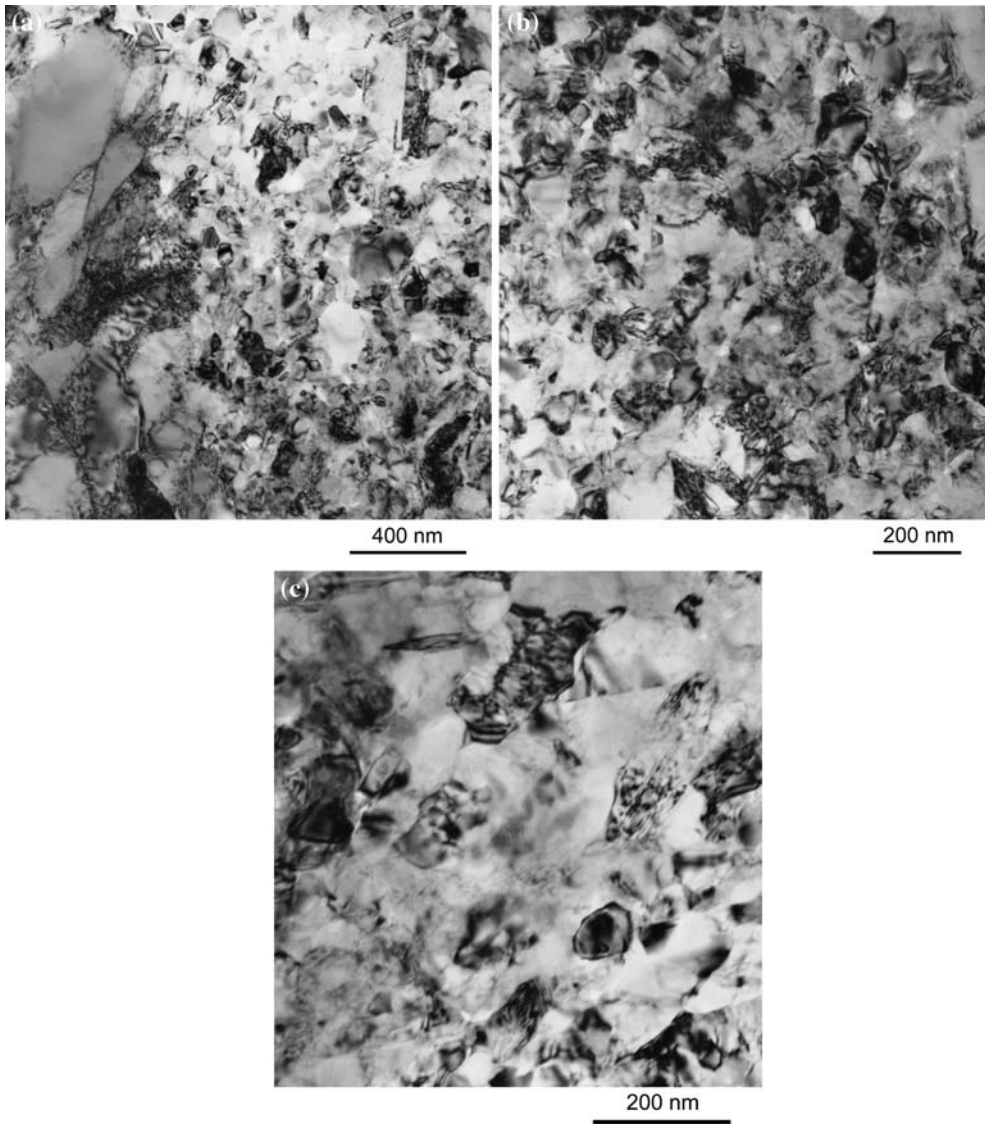

Fig. 8 Bright field TEM micrographs of the ECAE processed 130 nm Cu powder following different extrusion routes, (**a**) and (**b**) 2C, and (**c**) 2B. The foil normal is perpendicular to the longitudinal plane shown in Fig. 1

Two important conclusions were reached after the preliminary investigations on the nanoparticle consolidation. Firstly, any route that involves 180° rotations similar to route C, such as routes E and C′ at low number of passes (up to four) can not sufficiently eliminate the remnant porosity. The 180° rotation between passes leads to debonding along prior agglomerate boundaries. Therefore, route B with its orthogonal rotations between passes is the best choice among all at low number of passes. Secondly, it is believed that there are intrinsic length scales associated with ECAE shear during the extrusion of porous media that causes the observed flow lines in Fig. 6. In addition, the nanoparticle agglomeration and bimodal porosity distribution significantly affect this flow behavior and

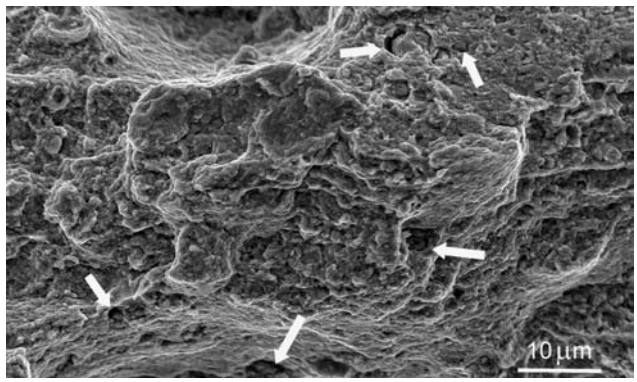

Fig. 9 Fracture surface of a tensile sample from the 130 nm copper powder consolidate (4E) [Courtesy of Ref. 66]. The arrows show potential sites for interparticle debonding

cause premature fracture in the resulting consolidates under tension (Fig. 9). To eliminate these effects and achieve better consolidation performance, one needs to break down the agglomerates as much as possible before the extrusion and decrease the agglomerate size range to levels less than the remnant macroporosity sizes observed in Fig. 6. In other words, the initial compact density should be increased as much as possible. The pores like the ones in Fig. 7, though, can be eliminated by just using the right processing route, i.e. route B. Alternatively, the same could be achieved by increasing the hydrostatic pressure levels with the application of a sufficient back pressure at the exit channel. This approach was recently proposed by Xia and Wu [73] and used for the consolidation of pure Al coarse particles at 100 °C. The tensile strength achieved was about 150 MPa and ductility was about 10%, which is, however, relatively low for an average resulting grain size of 7 μm.

Below, in Stages II and III, we have investigated the effect of initial compact density prior to ECAE on the final consolidation performance. This effort on breaking down and minimizing the effect of nanoparticle agglomeration resulted in some success supporting the arguments introduced above.

Microstructural evolution and tensile stress–strain response of consolidated Cu nanoparticles in Stages II and III

It is essential for a successful ECAE consolidation to have prior nanoparticle compacts with high initial density and a uniform density distribution, which can be obtained by breaking down the agglomerates. Higher initial compact density prior to ECAE should also permit larger consolidates and higher final material yield. Two methods were applied to manipulate the initial compact density and break down of agglomerates: (1) a hand pressing of nanoparticles incrementally using a 10 ksi hand-press in an inert gas environment, and (2) the application of hydrostatic pressures through CIPing, in the present case under 40 ksi.

Subsequent processing schedules involving route B were used for the further disintegration of the agglomerates. Several cans were ECAE processed mainly using route B up to 4 passes (4B) in both stages. In the 4B consolidates, at least 5 or more tensile experiments were conducted in each billet to determine the variation in the tensile response in different billets. Figure 10 shows the tensile stress versus strain curves with the highest and lowest tensile strength levels obtained from these samples. As can be clearly seen in the figure, this route permitted an extraordinary increase in the fracture strain to 6–7% for ultimate strength levels of around 750 MPa and above in both initially CIPed and hand pressed conditions. The average stress level is slightly higher in the CIPed case than the hand-pressed case, which can be attributed to better initial compaction in the former or to the slight difference in the initial average particle size. For comparison, the tensile stress–strain responses of the route B consolidate from Stage I, microcrystalline powder consolidate, and annealed Cu are also included. Clearly, the

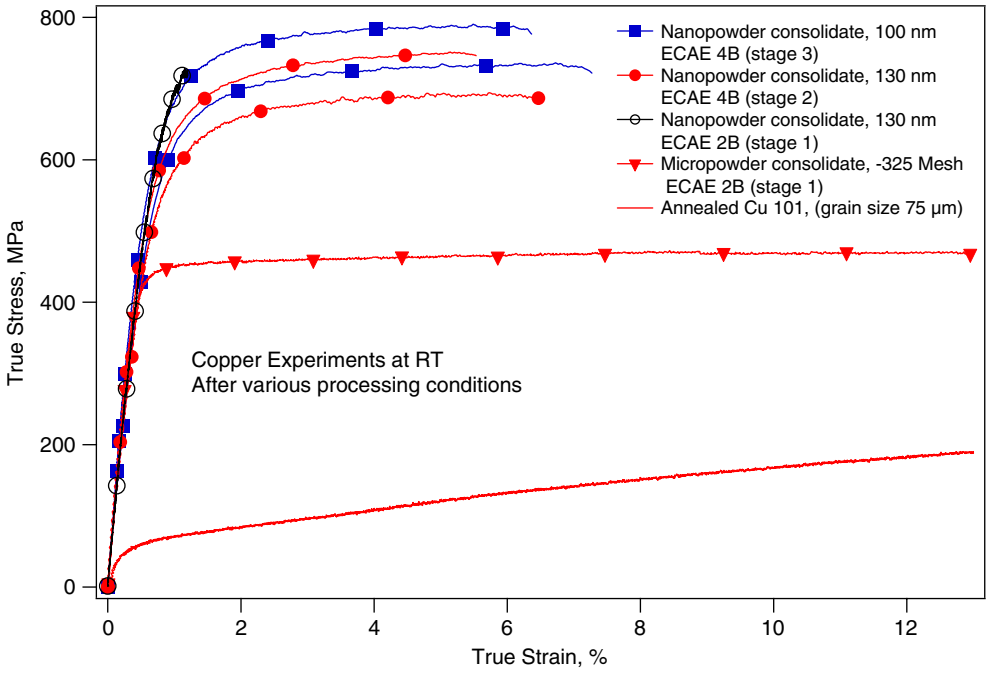

Fig. 10 Selected room temperature true stress–true strain responses of the ECAE consolidated Cu nanoparticles under tension demonstrating the effect of powder filling and compaction procedure prior to ECAE and initial particle size on the strength and tensile ductility levels. The curves with the same legends show the response of the tensile samples from different billets processed following the same ECAE route with the highest and the lowest tensile strength levels among more than 10 tensile samples from at least two different billets

Fig. 11 Image of the ECAE consolidated 100 nm Cu powder following route 4B with all dimensions in the centimeter range. Several tension samples were cut from the middle of the billet

attempt to break down the agglomerates and increase the initial compact density was shown to be successful in significantly improving the tensile ductility of Cu nanoparticle consolidates. The repeatability of the fracture strain levels are also notable since it shows that even if there might be some remnant porosity left in the consolidates, they are not as many and detrimental as the ones observed in Stage I. It can be speculated that even if cracks start to propagate from these pores, the material is ductile enough to suppress the crack propagation.

The material yield for Stages II and III was significantly higher due to the high initial compact density and less need for final compaction with ECAE. CIPing plus ECAE of nanoparticles using route 4B yielded near full density Cu samples with specimen dimensions of more than 1.5 cm in diameter and minimum lengths of 10 cm. One of the representative powder consolidates after CIPing and 4B ECAE is shown in Fig. 11 with about 18 mm diameter and 10 cm length. Table 3 summarizes the mechanical test results for the consolidated Cu nanoparticles in Stages II and III.

The TEM micrograph of the consolidated 100 nm Cu powder in Fig. 12 indicates the presence of a bimodal grain size distribution. The regions with considerably different average grain sizes are easily distinguishable as shown in the figure and their sizes are on the order of the prior agglomerate sizes. The areas with very fine grain sizes strengthen the material. It has been reported that the accumulation of dislocations is difficult in these fine grains as they are emitted from one grain-boundary segment and disappear at the adjacent one, leaving no dislocations inside the grain interior [100]. Figure 13 demonstrates such small grains in the present case. The ductility is thought to be mainly provided by the larger grains. Although the consolidation permitted to achieve some ductility (7.3%), we believe that it is possible to enhance the strain at fracture further as microstructures such as the one in Fig. 12 should provide larger strain levels since some of the large grain interiors appeared to be devoid of dislocations. This is an indicator that the material can sustain more plastic deformation if there is no catastrophic fracture. Indeed, Fig. 12 also demonstrates a non-uniform thickness of the TEM foil indicating a potential debonding line separating large prior agglomerates, shown by the arrows. This corroborates the idea of fracture initiation along prior inter-agglomerate interfaces.

Microstructural evolution and tensile stress–strain response of consolidated 316 L stainless steel nanoparticles

To demonstrate the applicability of ECAE nanoparticle consolidation for other materials, 316 L stainless steel (SS) nanoparticles was selected due to the similar crystal structure to Cu but with significantly different mechanical properties. Austenitic stainless steels are used in a broad range of industrial applications mainly because of their excellent corrosion resistance. However, their low yield strength often is a major drawback. Strengthening via nanocrystallization without significant loss of ductility could extend their use in industry. Compared to pure Cu, there are several additional issues in grain refinement, consolidation and resulting deformation response of nanocrystalline SS. These materials have low stacking fault energy, and

Table 3 Summary of the observed grain sizes and measured tensile properties in the Cu nanoparticles consolidated using ECAE at room temperature after filling the powder cans in vacuum, hand-pressing or CIPing, outgassing and sealing the cans

ECAE route	Case #	Powder size	Grain size (TEM)	Tension		
				σ_y (0.2%) (MPa)	σ_{UTS} (MPa)	ε_f (%)
2A*	23	130 nm	–	–	–	–
2B	24		–	457	441	0.7
4B	25		80–250 nm	584	749	6.0
4C′**	26		~250 nm and 40–80 nm	–	467	0.7
4B	27	100 nm	50–250 nm	605	790	6.2
2B	19	100 nm (SS)	100–200 nm	942	1030	3.9

Typical error bars from at least four companion specimens on σ_{UTS} were about ±15 MPa and about ±0.3% for the fracture strain. σ_y: 0.2% offset yield strength, σ_{UTS}: ultimate tensile strength, and ε_f: strain at fracture. *: It was not possible to obtain tension samples from this billet. **: The samples failed before any plastic deformation occurred

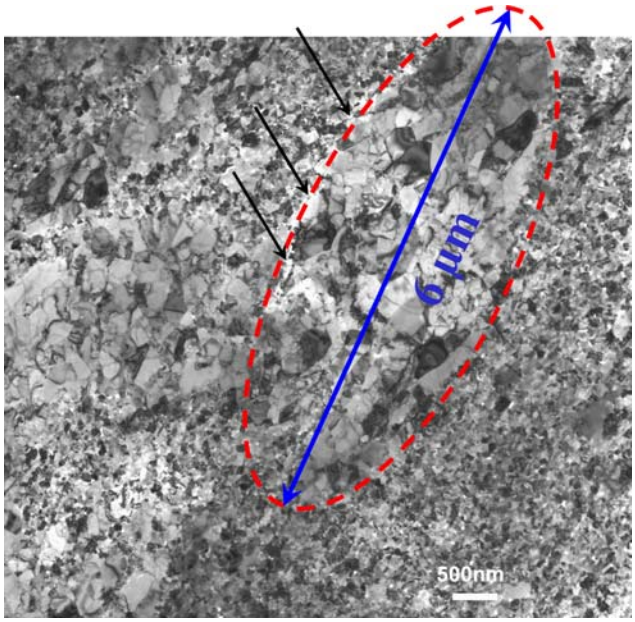

Fig. 12 Bimodal grain size distribution in the ECAE consolidated 100 nm Cu powder processed following route 4B. Some of the large grain interiors are nearly devoid of dislocations. The image also shows a line of preferential thinning of the TEM foil corresponding to a potential debonding site shown by the arrows

thus experience planar slip and twinning. Because of a small amount of carbon and nitrogen, static and dynamic strain aging can lead to additional complications in consolidation and deformation. On the other hand, the stability of nanostructures in SS will be improved over pure systems. Earlier results [61, 101] indicated that high strength levels are possible without sacrificing ductility in SS by combining grain refinement and twinning during ECAE at high temperatures. Therefore, SS was selected as a second and more challenging model alloy for consolidation.

The preliminary consolidations of SS nanoparticles with 100 nm average particle size were performed at 700 °C non-isothermally in an ECAE tool heated to 300 °C. The same preparation steps were used as Cu nanoparticles in Stage I except that the SS nanoparticles were vacuum outgassed at 130 °C for 8 h. The powder can was heated in a furnace for 30 min at 700 °C and transferred to the pre-heated tool in less than 5 s. This preliminary extrusion temperature was selected to minimize the effect of dynamic strain aging, which is usually operative around 400–600 °C and to eliminate the effect of twinning as much as possible. If the consolidation would be unsuccessful or if there would be some peculiarities in resulting consolidate microstructure or performance, it could have been difficult to understand the reasons because of the role of several factors. Clearly, minimizing the number of operative mechanisms makes the control of consolidation process much easier. ECAE at lower extrusion temperatures, though, will be investigated in the near future.

As can be seen in Fig. 14, an ultrahigh ultimate tensile strength of 1180 MPa was achieved in consolidated SS nanoparticles following route 2B having dimensions of 15 mm in diameter and 7 cm in length.

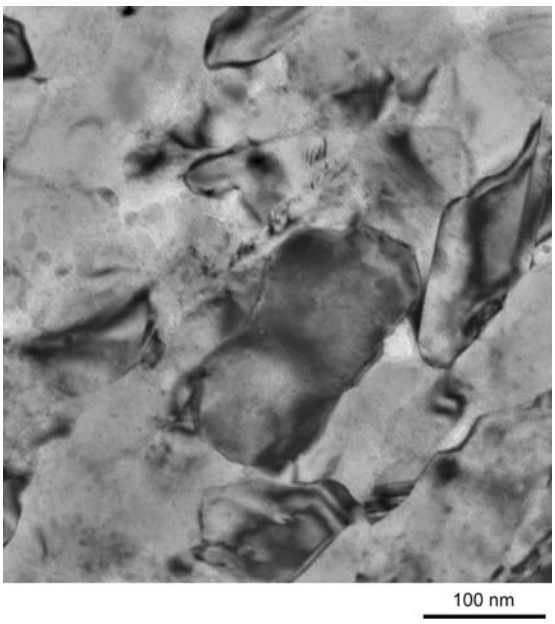

Fig. 13 Several nanograins with hardly any dislocation activity in the ECAE consolidated 130 nm Cu powder processed using route 4B at room temperature

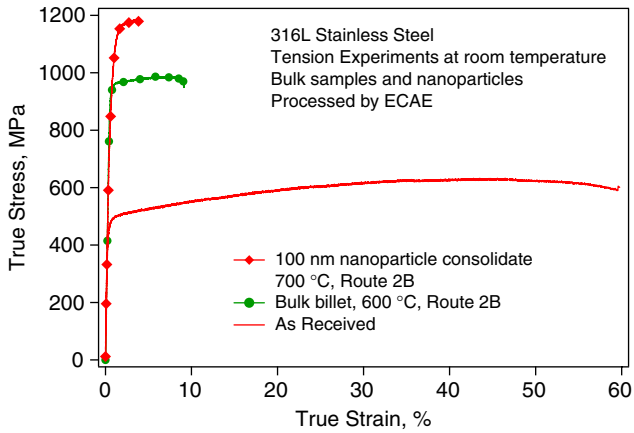

Fig. 14 Room temperature true stress–true strain response of the ECAE consolidated 100 nm 316L stainless steel particles following route 2B. For comparison, the tensile responses of the as-received coarse grained polycrystals and ultrafine grained 316 L stainless steel obtained using ECAE processing of the as-received material at 600 °C using route 2B are also shown

For comparison, the tensile responses of ECAE processed bulk 316L SS using route 2B at 600 °C (with an average final subgrain/grain size of about 200–300 nm) and as-received 316 L SS (average grain size of 45 μm) are also presented. The considerably higher strength level in the NC consolidates as compared to the one in the ECAE processed bulk sample can be clearly seen in the figure. However, such difference in strength levels cannot be solely attributed to grain refinement. TEM bright field images in Fig. 15 show that the grain sizes in the NC consolidate seem to be on the same order as that of the ECAE processed bulk sample. Grain sizes are similar as the microstructure of the consolidate seems to have partially recrystallized. However, mostly well-developed grain boundaries were observed in the NC consolidate as compared to less developed subgrain boundaries with low misorientation angles in the ECAE processed bulk material, and thus the strength level is considerably higher in the NC consolidate. Contamination of nanoparticles and higher interstitial content can also play an additional role in obtaining higher strength levels.

No deformation twinning activity was observed in the consolidated nanoparticles after two passes while considerable twin activity was evident even at 800 °C after one pass in the bulk samples [61]. The strain at fracture was 4% due to the same problem of inter-agglomerate debonding, which is a consequence of using only two passes. Further improvement in ductility is expected by using route 4B and by initially disintegrating and compacting the agglomerates through hand pressing or CIPing as in the Cu case.

What is the next step in the consolidation of nanoparticles using ECAE?

The ECAE process proved to be a very effective technique in the fabrication of *bulk* NC materials. However, further improvement in tensile ductility is needed. The inter-agglomerate debonding is shown to be the most detrimental effect on the final strain at fracture. Some fundamental questions need to be addressed regarding the formation of agglomerates and what the lower limit of their size is. To break down the agglomerates, we have used cold compaction prior to ECAE consolidation using hand-pressing or CIPing, which are shown to be effective. From the observed microstructures, further ductility improvements seem to be possible. Using higher CIPing pressures and applying higher number of passes in route B could provide such improvement by an additional break down of initial agglomerate sizes and further reduction in remnant porosity, respectively. One disadvantage of this processing approach is that it is a two-step process because of the involvement of CIPing. The application of a back pressure during ECAE can be an alternative eliminating the CIPing step, however, its effectiveness remains to be shown. This approach could also provide much higher hydrostatic pressure levels than what the can material imparts on the enclosed powder.

In the present study, we have not addressed the effects of the oxide layer present on the powder surface, oxygen or other interstitial contents, and powder size distribution. For the former, we have assumed from our previous studies [87, 88] that ECAE

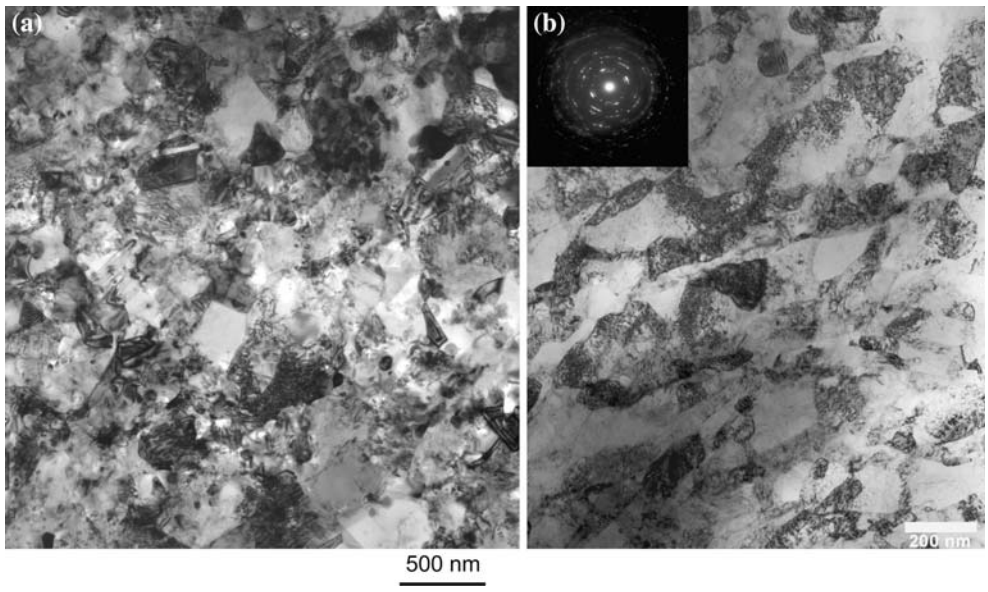

Fig. 15 Bright field TEM micrographs of (**a**) the consolidated 100 nm 316 L stainless steel powder after the consolidation using ECAE at 700 °C, and (**b**) the ultrafine grained bulk 316 L stainless steel billet processed by ECAE at 600 °C with initial coarse grains, both following route 2B

shear is capable of breaking the surface oxide layers easily. However, one needs to consider the effect of the size of broken oxide particles laying along the grain boundaries on the final ductility level. Perhaps, it might be necessary to apply higher number of passes to break down the size of these particles further and to reduce their effect on ductility. It is believed that nanometer size oxide particles along grain boundaries would significantly enhance the thermal stability of nanoparticle consolidates as shown in Al alloy consolidates [102].

Conclusions

In the present study, it was shown that ECAE can be a feasible method for fabricating bulk NC materials with all dimensions in the centimeter range. The mechanical properties and microstructural evolution of ECAE consolidated –325 mesh microcrystalline Cu particles, different size Cu nanoparticles and 100 nm stainless steel particles were investigated and correlated with the processing schedules. The ECAE consolidation of 100 and 130 nm Cu nanoparticles through route 4B, after the initial break down and compaction of the nanoparticle agglomerates using hand pressing or cold isostatic pressing, yielded excellent tensile properties. Maximum strength and strain levels of 790 MPa and 7.3%, respectively, were achieved in the Cu consolidates with bimodal grain size distribution. In the stainless steel nanoparticles, a maximum strength level of 1180 MPa with 4% tensile ductility was reached after the consolidation using route 2B at 700 °C. The inter-agglomerate debonding was shown to be the most important effect on the consolidation performance. It was argued that further improvement in tensile ductility could be possible if: (1) the nanoparticle agglomerates are initially broken further by using higher pressures during cold isostatic pressing, (2) more effective shearing is achieved by conducting higher number of ECAE passes in route B, and (3) high hydrostatic pressure levels accompany ECAE shear by the application of back pressure in the exit channel during ECAE.

Acknowledgements This work was supported by the Office of Naval Research under Grant No. N00014–05-1-0615 with Dr. Lawrence Kabacoff as program officer. Additional funding from National Science Foundation contract CMS 01-34554, Solid Mechanics and Materials Engineering Program, Directorate of Engineering, Arlington and Deutsche Forschungsgemeinschaft is gratefully acknowledged. The authors especially thank Mr. Larry Jones, Department of Energy Ames Laboratory, Materials Preparation Center, for his help for CIPing

References

1. Gleiter H (1989) Prog Mater Sci 33:223
2. Gleiter H (2000) Acta Mater 48:1
3. Yip S (1998) Nature 391:532
4. Yip S (2004) Nature Mater 3:11
5. Ma E (2004) Science 305:623
6. Milligan WW (2003) In: Milne I, Ritchie RO, Karihaloo B (eds) Comprehensive structural integrity. Elsevier Ltd., Oxford, p 529
7. Yamakov V, Wolf D, Phillpot SR, Mukherjee AK, Gleiter H (2004) Nature Mater 3:43
8. Weertman JR (2004) MRS Bulletin 29:616
9. Van Swygenhoven H, Weertman JR (2003) Scripta Mater 49:625
10. McFadden X, Mishra RS, Valiev RZ, Zhilyaev AP, Mukherjee AK (1999) Nature 398:684
11. Nieh TG, Wadsworth J (1991) Scripta Metall Mater 25:955
12. Siegel RW, Fougere GE (1995) Nanostruct Mater 6:205
13. Youssef KM, Scattergood RO, Murty KL, Koch CC (2004) Appl Phys Lett 85:929
14. Koch CC (2003) Scripta Mater 49:657
15. Scattergood RO, Koch CC (1992) Scripta Metall Mater 27:1195
16. Carsley JE, Fisher A, Milligan WW, Aifantis EC (1998) Metall Mater Trans A 29:2261
17. Erb U (1995) Nanostruct Mater 6:533
18. Erb U, Palumbo G, Szpunar B, Aust KT (1997) Nanostructured Mater 9:261
19. Van Swygenhoven H, Derlet PM, Froseth AG (2004) Nature Materials 3:399
20. Froseth A, Van Swygenhoven H, Derlet PM (2004) Acta Mater 52:2259
21. Kumar KS, Van Swygenhoven H, Suresh S (2003) Acta Mater 51:5743
22. Derlet PM, Van Swygenhoven H (2002) Scripta Mater 47:719
23. Van Swygenhoven H (2002) Science 296:66
24. Cheng S, Spencer JA, Milligan WW (2003) Acta Mater 51:4505
25. Wang YM, Chen MW, Zhou FH, Ma E (2002) Nature 419:912
26. Chen MW, Ma E, Hemker KJ, Sheng HW, Wang YM, Cheng XM (2003) Science 300:1275
27. Ma E (2003) Nature Mater 2:7
28. Wang YM, Ma E (2004) Acta Mater 52:1699
29. Weertman JR (2002) Mater Sci Forum 386:519
30. Koch CC (1993) Nanostructure Mater 2:109
31. Masumura RA, Hazzledine PM, Pande CS (1998) Acta Mater 46:4527
32. Weertman JR, Farkas D, Hemker K, Kung H, Mayo M, Mitra R, van Swygenhoven H (1999) MRS Bull 24:44
33. Ma E (2003) Scripta Mater 49:663
34. Perepezko JH, Hebert RJ, Wilde G (2004) Mat Sci Eng A 375–77:171
35. Inoue A (1999) Prog Mater Sci 43:365
36. Gaffet E, Bernard F, Niepce J-C, Charlot F, Gras C, LeCaer G (1999) Mater J Chem 9:305
37. Gaffet E, Bernard F (2002) Annales De Chimie-Science Des Materiaux 27:47
38. Rawers J, Slavens G, Govier D, Dogan C, Doan R (1998) Metall Mater Trans A 27:3126
39. Hayes RW, Witkin D, Zhou F, Lavernia EJ (2004) Acta Mater 52:4259
40. Hayes RW, Rodriguez R, Lavernia EJ (2001) Acta Mater 49:4055

41. He L, Ma E (1995) Mater Sci Eng A 204:240
42. Rawers J (1999) Nanostructured Mater 11:513
43. Hida M, Asai K, Takemoto Y, Sakakibara A (1996) Mater Trans JIM 37:1679
44. Baláž P, Godočíková E, Kril'ová L, Lobotka P, Gock E (2004) Mater Sci Eng A 386:442
45. Cheng S, Ma E, Wang YM, Kecskes LJ, Youssef KM, Koch CC, Trociewitz UP, Han K (2005) Acta Mater 53:1521
46. Sanders PG, Eastman JA, Weertman JR (1997) Acta Mater 45:4019
47. Youngdahl CJ, Sanders PG, Eastman JA, Weertman JR (1997) Scripta Mater 37:809
48. Shaik GR, Milligan WW (1997) Metall Mater Trans A 28:895
49. Li HQ, Ebrahimi F (2004) Appl Phys Lett 84:4307
50. Li HQ, Ebrahimi F (2003) Acta Mater 51:3905
51. Legros M, Elliott BR, Rittner MN, Weertman JR, Hemker KJ (2000) Phil Mag A80:1017
52. Kumar KS, Suresh S, Chisholm MF, Horton JA, Wang P (2003) Acta Mater 51:387
53. Yoo SH, Sudarshan TS, Sethuram K, Subhash G, Dowding RJ (1999) Nanostructure Mater 12:23
54. Srivatsan TS, Ravi BG, Naruka AS, Riester L, Yoo S, Sudarshan TS (2001) Mat Sci Eng A 311:22
55. Wan J, Duan RG, Mukherjee AK (2005) Scripta Mater 53:663
56. Kim HC, Shon IJ, Garay JE, Munir ZA (2004) Int J Refractory Metal Hard Mater 22:257
57. Lowe TC, Valiev RZ (2000) JOM 52 No 4:27
58. Valiev RZ, Islamgaliev RK, Alexandrov IV (2000) Prog Mater Sci 45:103
59. Valiev RZ, Alexandrov IV, Zhu YT, Lowe TC (2002) J Mater Res 17:5
60. Ferrasse S, Segal VM, Hartwig KT, Goforth RE (1997) Metall Mater Trans A 28:1047
61. Yapici GG, Karaman I, Luo ZP (2004) J Mater Res 19:2268
62. Yapici GG, Karaman I, Luo ZP, Rack H (2003) Scripta Mater 49:1021
63. Iwahashi Y, Horita Z, Nemoto M, Langdon TG (1998) Acta Mater 46:3317
64. Furukawa M, Horita Z, Nemoto M, Langdon TG (2001) J Mater Sci 36:2835
65. Xu C, Furukawa M, Horita Z, Langdon TG (2004) J Alloys and Compounds 378:27
66. Haouaoui M, Karaman I, Maier HJ, Hartwig KT (2004) Metall Mater Trans A 35:2935
67. Zhu YT, Lowe TC, Langdon TG (2004) Scripta Mat 51:825
68. Delo DP, Semiatin SL (1999) Metall Mater Trans A 30:2473
69. Sergueeva AV, Song C, Valiev RZ, Mukherjee AK (2003) Mater Sci Eng A 339:159
70. Liao XZ, Zhao YH, Zhu YT, Valiev RZ, Gunderov DV (2004) J Appl Phys 96:636
71. Hartwig KT, Karaman I, Haouaoui M, Mathaudhu SN (2003) In: Senkov ON (ed) Proceedings of the 2003 NATO Advanced Research Workshop on Metallic Materials with High Structural Efficiency Kiev, Ukraine, September 6–13, 2003, Kluwer Academic Publishers, the Netherlands, 2004, p 91
72. Haouaoui M, Karaman I (2003) Powder materials: current research and industrial practices III. In: FDS Marquis (ed) Proceedings of the international symposium on powder materials: current research and industrial practices iii, Materials Science & Technology 2003 meeting, Chicago, IL, November 9–12, 2003, edited by (TMS, Warrendale, 2003) p. 125
73. Xia K, Wu X (2005) Scripta Mater 53:1225
74. Senkov ON, Senkova SV, Scott JM, Miracle DB (2005) Mater Sci Eng A 393:12
75. Leipert S (1999) The influence of equal channel angular extrusion on texture evolution in pure tantalum. MS Thesis, Texas A&M University, 1999
76. Gibbs MA, Hartwig KT, Cornwell LR, Goforth RE, Payzant EA (1998) Scripta Mater 39:1699
77. Haouaoui M, Hartwig KT, Payzant EA (2005) Acta Materialia 53:801
78. Segal V, Goforth RE, Hartwig KT (1995) Texas A&M University, US Patent No 5,400,633
79. Segal V (1996) US Patent No 5,513,512
80. Segal V, Segal L (1996) US Patent No 5,600,989
81. Furukawa M, Iwahashi Y, Horita Z, Nemoto M, Langdon TG (1998) Mater Sci Eng A 257:328
82. Parasiris A, Hartwig KT, Srinivasan MN (2000) Scripta Mater 42:875
83. Parasiris A, Hartwig KT (2000) Int J Refract Metals Hard Mater 18:23
84. Pearson J (1997) Consolidation of Al6061 Powder by ECAE. MS Thesis, Texas A&M University, 1997
85. Zapata H (1998) Application of Equal Channel Angular Extrusion to Consolidate Aluminum 6061 Powder. MS Thesis, Texas A&M University
86. Hartwig KT, Zapata H, Parasiris A, Mathaudhu SN (2001) In: Marquis FDS, Thadhani N, Barrera EV (eds) Proceedings of the powder materials: current research and industrial practices symposium, (2001) TMS Publications 211
87. Karaman I, Robertson J, Im J-T, Mathaudhu SN, Luo ZP, Hartwig KT (2004) Metall Mater Trans A 35:247
88. Robertson J, Im J-T, Karaman I, Hartwig KT, Anderson IE (2002) J Non-Crystal Solids 317:144
89. Hartwig KT, Chase G, Belan J (2003) IEEE Trans Appl Superconductivity 13 N°2:3548
90. Witkin D, Lee Z, Rodriguez R, Nutt S, Lavernia EJ (2003) Scripta Mater 49:297
91. Zhang YW, Liu P, Lu C (2004) Acta Mater 52:5105
92. Champion Y, Langlois C, Guerin S-Mailly, Langlois P, Bonnentien J-L, H MJ (2003) Science 300:310
93. Hague DC, Mayo MJ (1999) J Am Ceram Soc 82:545
94. Graneau P (1987) Phys Lett 120:77
95. Haouaoui M (2006) An investigation of bulk nanocrystalline copper fabricated via severe plastic deformation and nanoparticle consolidation using equal channel angular extrusion. PhD Thesis, Texas A&M University, 2006
96. Smallman RE, Westmacott KH (1957) Phil Mag 2:669
97. Warren BE In: X-ray Diffraction, Dover, New York, NY, Chap 13
98. ASTM Standard C20–92, ASTM, Philadelphia, PA, 15 (1996) 5
99. Haouaoui M, Karaman I, Maier HJ (2006) Acta Materialia 54:5477
100. Liao XZ, Zhou F, Lavernia EJ, Srinivasan SG, Baskes MI, He DW, Zhu YT (2003) Appl Phys lett 83:632
101. Karaman I, Yapici GG, Chumlyakov YI, Kireeva IV (2005) Mater Sci Eng A 410:243
102. Han BQ, Zhang Z, Lavernia EJ (2005) Phil Mag Lett 85:97